Acoustic wave propagation in the Sun

By T. Hartlep AND N. N. Mansour

1. Motivation and objectives

The evolution of the solar interior is a challenging and fascinating subject in physics and is actively studied theoretically, numerically, and observationally. Numerical simulations are becoming increasingly sophisticated. Realistic simulations of the three-dimensional compressible magneto-hydrodynamic (MHD) equations have been performed for the shallow upper layer of the convection zone (Stein & Nordlund 2000). They capture convective structures on the granular scale. Acoustic waves are included in these fully compressible simulations. As a result, oscillation spectra obtained from such simulations are in good agreement with solar measurements. Unfortunately, simulations of this type are not expected to be feasible for deep domains or for the whole sun anytime soon due to the enormous computational requirements. However, we know that as we go deeper from the surface of the sun, the turbulent flow structures become larger, and the Mach number decreases. In fact, for the most part, the solar interior convective motions are much slower than the speed of sound with a Mach number estimated to be of order 10^{-2}. It is then possible to simulate the flow field by using the anelastic approximation proposed by Gough (1969) and later adapted for the solar case by Gilman & Glatzmaier (1981), instead of using the fully compressible equations. The approximation retains the effects of stratification but filters out the much faster acoustic waves.

On the other hand, acoustic waves should not be forgotten completely. Helioseimology, the study of solar oscillations, has been a very active field in recent years and has made a profound impact on our understanding of the structure and dynamics of the sun. For instance, helioseismic inferences are able to measure the differential rotation of the sun. However, helioseismic inversion techniques are based on simplified models of solar oscillations, which have not been tested for validity. For instance, global helioseismology assumes that the sun is axisymmetric, but the real sun is not axisymmetric. The consequences of the real, non-axisymmetric 3D structures for the oscillation properties, *e.g.* frequencies, line-width, amplitudes, are not well known. Three dimensional numerical simulations of acoustic wave propagation in the sun could test some of the assumptions currently used and could provide artificial data for testing and calibrating helioseimic inversion methods (Werne, Birch & Julien 2004). This project tries to make the first steps in this direction.

2. Numerical method

In the following we summarize the mathematical model and the numerical method. We briefly introduce the equations, the boundary conditions, the time differencing method, and the spatial discretization. We also take a closer look at the coordinate singularities arising in spherical coordinates and discuss their treatment in the numerical method.

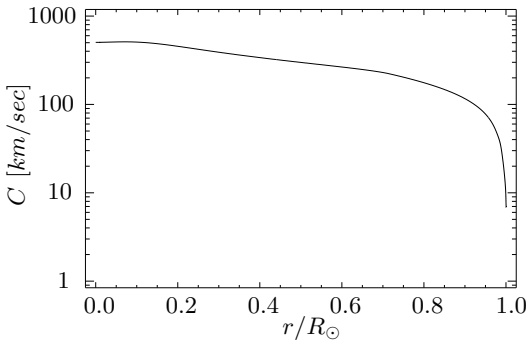

FIGURE 1. Speed of sound in a standard solar model as a function of radius (Christensen-Dalsgaard 1996).

2.1. *Basic equations and boundary conditions*

We start with the simplest problem one can imagine. Of the various types of helioseismic oscillations (p-, f-, and g-modes, *i.e.* pressure, surface gravity, and internal gravity waves), we consider only the pressure waves and neglect any convection in the sun. The governing equation is therefore a simple wave equation of the form:

$$\partial_t^2 \rho = \Delta(C^2 \rho), \tag{2.1}$$

which can be written as a system of two first order equations:

$$\partial_t \rho = -\Phi \tag{2.2}$$

$$\partial_t \Phi = -\Delta(C^2 \rho). \tag{2.3}$$

ρ denotes the density variations with respect to the background, Δ is the Laplacian operator, and C is the sound speed which itself is a function of space. Even though we neglect the direct effects of the flow field on the waves, the effects of spatial temperature variations are included through the change of sound speed. A non-reflecting boundary condition is imposed at the upper radial boundary by adding a buffer layer. The equations are modified by adding damping terms:

$$\partial_t \rho = -\Phi - \sigma \rho \tag{2.4}$$

$$\partial_t \Phi = -\Delta(C^2 \rho) - \sigma \Phi, \tag{2.5}$$

where σ is the damping coefficient. It is independent of time and is set to be zero in the interior, and it increases smoothly into the buffer layer. Recasting the equations by using an integrating factor and applying the staggered scheme for the time differencing results in

$$\rho^{n+1} = \exp(-\sigma h)\rho^n - \exp(-\sigma h/2)\Phi^{n+1/2} \tag{2.6}$$

$$\Phi^{n+3/2} = \exp(-\sigma h)\Phi^{n+1/2} - \exp(-\sigma h/2)\Delta(C^2\rho)^{n+1}, \tag{2.7}$$

where $h = t_{n+1} - t_n$ is the time step.

2.2. *Spatial discretization*

The spatial resolution requirements vary considerably with radius due to the strong radial variation of the sound speed (see Fig. 1). Ideally, we would like to change both the radial

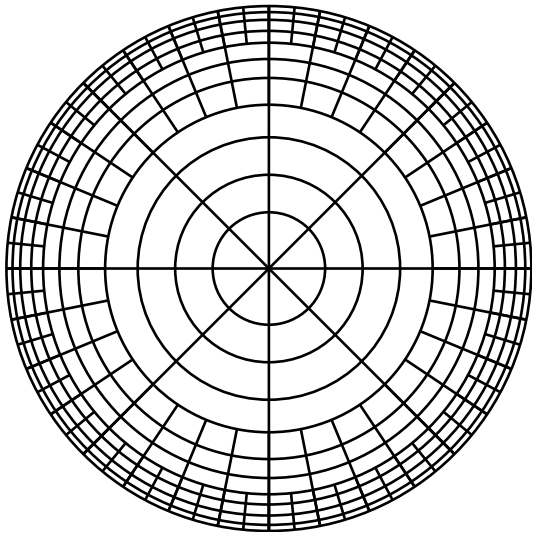

FIGURE 2. Illustration of an optimized grid for solar simulations. The radial spacing of knot points is chosen according to the local sound speed such that the travel time for the waves from one knot point to the next is approximately the same anywhere in the domain. For the same reason, it is also advantageous to drop spherical modes as we go deeper into the sun in order to decrease the angular resolution.

and angular resolution as we go deeper into the sun (see figure 2). This is possible by using a B-spline method (Loulou, Moser, Mansour & Cantwell 1997; Kravchenko, Moin & Shariff 1999; Hartlep & Mansour 2004) in radial direction and spherical harmonics $Y^{l,m}$ for the angular dependencies, *i.e.* we use an expansion in the form

$$\rho^n(r,\theta,\phi) = \sum_{l,m,j} \hat{\rho}^n_{l,m,j} Y^{l,m}(\theta,\phi) B^j(r) \tag{2.8}$$

$$\Phi^n(r,\theta,\phi) = \sum_{l,m,j} \hat{\Phi}^n_{l,m,j} Y^{l,m}(\theta,\phi) B^j(r). \tag{2.9}$$

The B-splines $B^j(r)$ are piecewise polynomials of a chosen order with local support (see Fig. 3). Analogous to Hartlep & Mansour (2004) we plug the expansions in (2.6) and (2.7) and project onto a B-spline $B^i(r)$. The result is a linear set of equations for the expansion coefficients at the next time step:

$$\sum_j \hat{\rho}^{n+1}_j \mathcal{M}^{i,j} = \sum_{j,k} \eta_j \hat{\rho}^n_k \mathcal{N}^{i,j,k} - h \sum_{j,k} \zeta_j \hat{\Phi}^{n+1/2}_k \mathcal{N}^{i,j,k} \tag{2.10}$$

$$\sum_j \hat{\Phi}^{n+3/2}_j \mathcal{M}^{i,j} = \sum_{j,k} \eta_j \hat{\Phi}^{n+1/2}_k \mathcal{N}^{i,j,k} - h \sum_{j,k} \zeta_j \widehat{c^2 \rho_k}^{n+1} \mathcal{R}^{i,j,k}_l. \tag{2.11}$$

η_j and ζ_j are the B-spline coefficients for the damping terms. The equations are solved by inverting the matrix $\mathcal{M}^{i,j}$. All matrix elements appearing in the above equations are constant and are computed and stored at the beginning of a simulation. They depend only on the B-spline order and the choice of radial knot points, except for $\mathcal{R}^{i,j,k}_l$, which

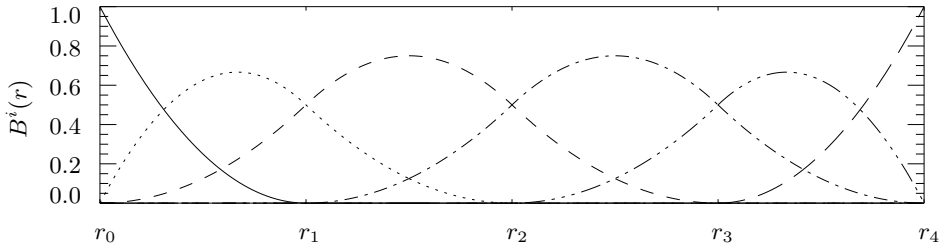

FIGURE 3. Second-order B-splines defined on a sets of 5 knot points. Solid, dotted, dashed, dash-dotted, dash-dot-dotted and long-dashed lines denote splines $B^1, \ldots, B^6$, respectively.

also depends on the spherical harmonic degree l. The matrix elements are given by:

$$\mathcal{M}^{i,j} = \int B^i(r) B^j(r) dr, \tag{2.12}$$

$$\mathcal{N}^{i,j,k} = \int B^i(r) B^j(r) B^k(r) dr, \tag{2.13}$$

$$\mathcal{R}_l^{i,j,k} = \left(\mathcal{O}^{i,j,k} + 2\mathcal{P}^{i,j,k} - l(l+1)\mathcal{Q}^{i,j,k}\right), \tag{2.14}$$

$$\mathcal{O}^{i,j,k} = \int B^i(r) B^j(r) \frac{\partial^2}{\partial r^2} B^k(r) dr, \tag{2.15}$$

$$\mathcal{P}^{i,j,k} = \int \frac{1}{r} B^i(r) B^j(r) \frac{\partial}{\partial r} B^k(r) dr, \tag{2.16}$$

$$\mathcal{Q}^{i,j,k} = \int \frac{1}{r^2} B^i(r) B^j(r) B^k(r) dr. \tag{2.17}$$

Since the B-spline functions have local support, all matrices are sparsely populated band matrices with k super- and k sub-diagonals. k is the polynomial order of the B-splines. Computing the inverse of $\mathcal{M}^{i,j}$ is therefore computationally inexpensive.

2.3. *Center singularity*

The use of spherical coordinates, though appropriate for a spherical body, comes with the problem of coordinate singularity that needs to be treated correctly. These singular points are the polar axis ($\theta = 0$) and the center of the sphere ($r = 0$). Using spherical harmonics for the angular dependencies ensures that all solutions are smooth near the poles. One way to avoid problems from the center singularity is to simply cut out the central region in the simulation. Simulating to whole sphere, however, requires some adjustments to the numerical method as we will see in the following. We start with a scalar field expanded in spherical harmonics:

$$f(r, \theta, \phi) = \sum_{l,m} \hat{f}_{l,m}(r) Y^{l,m}(\theta, \phi), \tag{2.18}$$

and apply, as in the acoustic wave equation, the Laplacian operator:

$$\Delta f(r, \theta, \phi) = \Delta \sum_{l,m} \hat{f}_{l,m}(r) Y^{l,m}(\theta, \phi) = \sum_{l,m} Y^{l,m}(\theta, \phi) \mathcal{L}_l \hat{f}_{l,m}(r), \tag{2.19}$$

where

$$\mathcal{L}_l = \frac{\partial^2}{\partial r^2} + \frac{2}{r}\frac{\partial}{\partial r} - \frac{l(l+1)}{r^2}. \tag{2.20}$$

The problem lies with the $1/r$ and $1/r^2$ terms as r goes to zero. Not all smooth radial functions $\hat{f}_{l,m}(r)$ have smooth Laplacians at $r = 0$, as the simple example $\hat{f}_{l,m}(r) = 1$ illustrates. What we need is a condition for the radial functions that insures that the Laplacian remains regular at the center of the sphere.

To derive such a constraint, we expand $\hat{f}_{l,m}(r)$ in a Taylor series about the origin $r = 0$

$$\hat{f}_{l,m}(r) = \sum_{p=0}^{\infty} a_{l,m,p} r^p \,, \tag{2.21}$$

and we apply the Laplacian operator to each power individually:

$$\mathcal{L}_l r^p = (p-l)(p+l+1) r^{p-2}. \tag{2.22}$$

For the case $p-2 < 0$, the derivative remains bounded only if the prefactor vanishes (*i.e.* $p = l$). (2.22) is always a regular expression if, on the other hand, $p - 2 \geq 0$. Applying the Laplacian operator n-times, such that $q = p-2n$ is greater or equal to zero, but $q-2$ is less than zero, yields:

$$(\mathcal{L}_l)^n r^p = c_{p,n} r^{p-2n} \tag{2.23}$$

with

$$c_{p,n} = \sum_{i=1}^{n} \big((p-2i+2)-l\big)\big((p-2i+2)+l+1\big). \tag{2.24}$$

If we now apply the operator one more time, we have:

$$(\mathcal{L}_l)^{n+1} r^p = c_{p,n}(q-l)(q+l+1) r^{q-2} \qquad \text{with } \; q = p-2n, \tag{2.25}$$

and the exponent becomes negative. The expression therefore remains regular at the center only if the prefactor vanishes, which is the case if $q = l$, and, correspondingly, $p = l+2n$. In other words, the functional behavior near $r = 0$ of any valid radial function can be written in the form

$$\hat{f}_{l,m}(r) = \sum_{i=0}^{\infty} a_{i,l,m} r^i \qquad \text{with } a_{i,l,m} = 0 \;\forall\; i \neq 2n+l \;(n \in \quad). \tag{2.26}$$

As we have seen, only functions that can be expressed in this way ensure a smooth field at the origin. It can be shown that this constraint is not only necessary but sufficient in that the number of degrees of freedom in an expansion in spherical harmonics with radial functions of the form (2.26) equals the number of degrees of freedom in a corresponding expansion in Cartesian coordinates x, y, and z where there is no coordinate singularity to begin with.

Since in our numerical method all radial functions are expressed in terms of basis splines, we need to translate the above constraint into a constraint for the corresponding expansion coefficients. (2.26) applies only for the behavior near $r = 0$, and we can limit the analysis to the very first interval $I_1 = [r_0, r_1]$. Omitting the indices l and m for clarity, the B-spline expansion for that interval reads:

$$\hat{f}(r) = \sum_{i=1}^{k+1} \alpha_i B^i(r) \qquad (r \in I_1). \tag{2.27}$$

Here, we ignore higher B-splines ($i > k+1$), since they are identically zero in I_1. The B-spline functions themselves are piecewise polynomials with fixed polynomial coefficients

$\beta_{i,j}$ such that $\hat{f}(r)$ in the first interval is given by an expansion

$$\hat{f}(r) = \sum_{i=1}^{k+1} \sum_{j=0}^{k} \alpha_i \beta_{i,j} r^j \qquad (r \in I_1). \tag{2.28}$$

On the other hand, $\hat{f}(r)$ must also satisfy (2.26), which leads to a linear equation of the form

$$\sum_{i=1}^{k+1} \alpha_i \beta_{i,j} = a_j \qquad (j \in [0,k]). \tag{2.29}$$

In general, this equation is under-determined, since the only *a priori* knowledge we have about the a_i's is the constraint from (2.26) (*i.e.* $a_i = 0 \; \forall \; i \neq 2n + l \; , n \in \quad$). (2.29) is solved symbolically for the α_i's, and the resulting constraints are then incorporated into the B-spline method in the same way that boundary conditions are implemented, see Hartlep & Mansour (2004).

3. Results

To validate this new numerical code, the first goal was to reproduce what is already known about the acoustic field within the sun. One of the most important properties is the existence of a discrete spectrum of standing oscillation modes. Acoustic waves are created mainly by the turbulent flow close below the surface and, due to the sharp drop in the sound speed near the surface of the sun, waves are, depending on their wavelength, partially or totally reflected back into the interior. The sun becomes a resonating cavity.

To account for the random sound sources, we consider the following simple setup. We excite waves by adding a random source term in the ρ equation. At each time step and for each spherical harmonic mode (l,m) a Gaussian pulse at radial position $r = 0.9R_\odot$, with a width of $\sigma = 0.02R_\odot$ and a random amplitude, is added to the equation. In the case we consider here, we use the radially symmetric sound speed from the standard solar model shown earlier in Fig 1, there is no coupling between different spherical harmonic modes. And, since we are only interested in normalized oscillation spectra, we can force each mode with equal strength. After a transition period, the input of acoustic energy from the source term and the loss through the surface reach an equilibrium, and the sound field is in a statistically steady state.

The simulation parameters are as follows. We consider only spherical harmonic degrees from $l = 0$ to $l = 42$ and do not drop radial modes with radius, even though this capability in available in the code. In the radial direction, B-splines of order 4 are used, generated from a set of 125 knot points. The spacing of the knots is varied over the radius and is proportional to the local sound speed: small at the top and large in the interior. The travel time of an acoustic wave from one knot point to the next is therefore approximately the same anywhere in the domain. Instead of treating the center singularity in the way explained in section 2.3, here we leave out the center completely and only consider radii from $0.2 \times 10^8 m$ to $7.2 \times 10^8 m$. This, at least in this uncoupled case, only affects modes with very low harmonic degree, since those are the only ones that reach deep enough into the interior. Buffer layers both at the top (reaching down to about $6.9 \times 10^8 m$, slightly below the solar surface $R_\odot \approx 6.96 \times 10^8 m$) and at the lower end of the radial domain (going up to about $2 \times 10^8 m$) are used. A time step of $h = 0.25s$ is used, which is smaller than the travel time for a wave between any two neighboring knot points. The

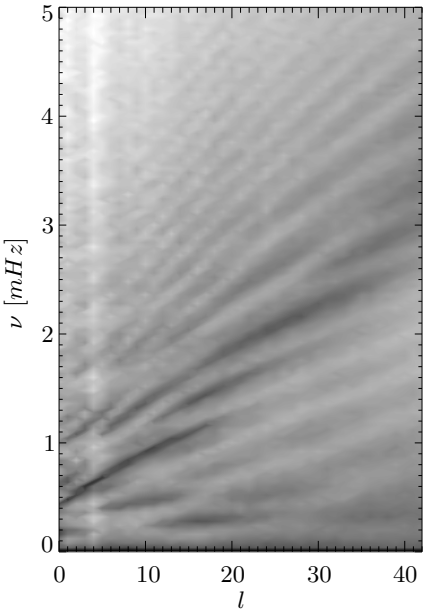

FIGURE 4. Normalized acoustic power spectrum as a function of spherical harmonic degree l, averaged over all azimuthal numbers m.

simulation is run for a total of 800,000 time steps to provide a reasonable amount of data for statistical analysis.

The power spectrum of the acoustic modes computed from the simulation is shown in Fig. 4. Individual spectra for each spherical harmonic degree l and azimuthal number m are computed from time series of the amplitude of a B-spline located at about $0.9R_\odot$. The spectra are normalized such that the sum over all frequencies equals to one, and are then averaged over azimuthal number m. As seen in the figure, bands of oscillation modes with frequencies increasing with spherical harmonic degree l are present. This qualitatively agrees with spectra from theoretical models and actual measurements (see e.g. Rhodes *et al.* (1997); Christensen-Dalsgaard (2002)), though there is a slight abnormality at very low l, notably $l = 4$. As mentioned earlier, this might be related to a shading effect that the inner buffer layer may have on the low-l modes. Quantitative comparisons of the observed frequencies have not been made yet, but the modes seen in the spectrum are definitely in the correct range of frequencies. More precise comparisons are the next step in our investigation.

We mentioned earlier that modes with low harmonic degree penetrate deep into the interior, while modes with higher harmonic degree are mostly confined to the outer part of the sun. Figure 5, which shows a snapshot of the contributions of different spherical harmonic degree to the total wave field, supports that claim. At a low degree of $l = 5$, a substantial amplitude is found even close to the lower damping layer ($0.2R_\odot$), while higher l-modes have already decayed at a much larger radius. This property can be exploited to drop unnecessary spherical modes at low radii.

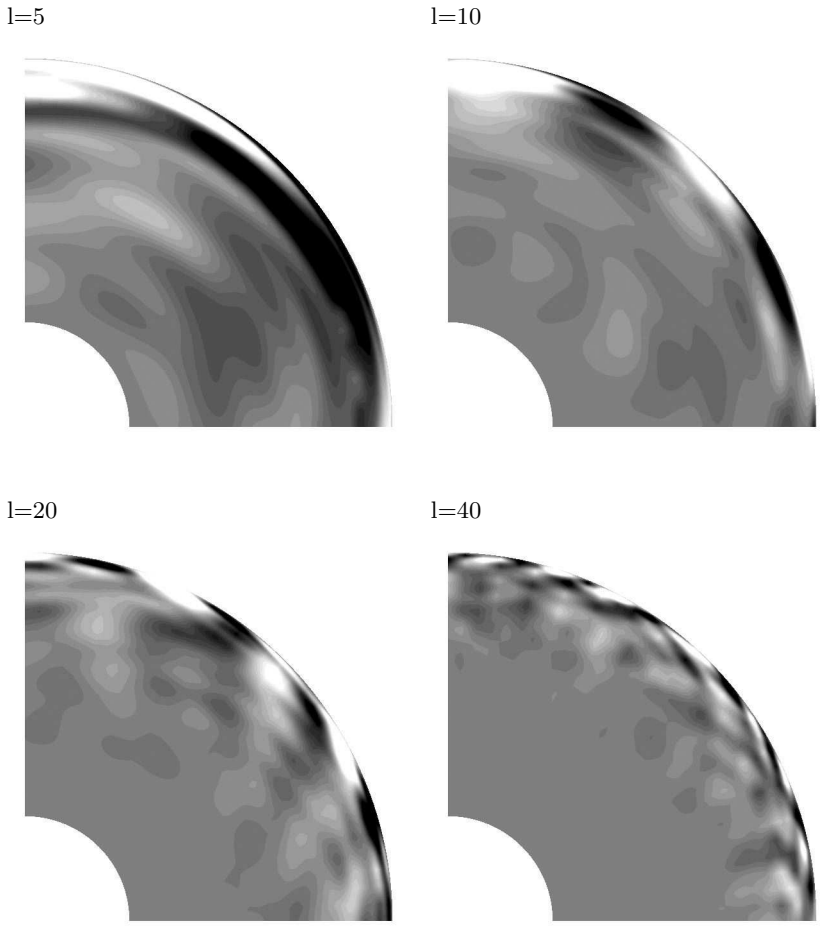

FIGURE 5. Snapsshot of the density variations in the acoustic field from a randomly forced simulation as explained in the text. Shown are the contributions of modes with spherical harmonic degree $l = 5, 10, 20$ and 40. The scale is different for each panel due to the different amplitude of each mode, but white always corresponds to the lowest and black to the highest value in that l-mode. Buffer layers are not shown.

4. Future work

We have presented a method for simulating the propagation of acoustic pressure waves in a three-dimensional model of the sun in spherical coordinates. Spatial discretization is by means of spherical harmonic functions and B-splines. A staggered Yee scheme is used for the time differencing. Results for a simple simulation with radially symmetric sound speed and without any flow field have been presented.

The current model is too simple to be of much practical use, but it demonstrates the feasibility of such global acoustic wave simulations. Modifications to the equations are planned to incorporate important factors such as the effects of convection and differential rotation on the waves. More accurate modeling of the acoustic sources is another problem that needs to be addressed. One idea is to use statistical data extracted from compressible flow simulations of the upper part of the sun's convective layer, where the sources are

primarily situated. Not only will we be able to learn more about solar oscillation, but these future simulations can be used to test and to help improve current helioseismic inversion techniques.

REFERENCES

Christensen-Dalsgaard, J. 1996 The current state of solar modeling. *Science* **272**, 1286–1292.

Christensen-Dalsgaard, J. 2002 Helioseismology. *Rev. Mod. Phys.* **74**, 1073–1129.

Gilman, P. & Glatzmaier, G. A. 1981 Compressible convection in a rotating spherical shell. I. Anelastic equations. *Astrophys. J. Suppl.* **45**, 335–388.

Gough, D. O. 1969 The anelastic approximation for thermal convection. *J. Atmos. Sci.* **26**, 448–456.

Hartlep, T. & Mansour, N. N. 2004 Solar convection simulations using a B-spline method. *Annual Research Briefs 2004*. Center for Turbulence Research, NASA Ames/Stanford Univ.

Kravchenko, A. G., Moin, P. & Shariff, K. 1999 B-spline method and zonal grids for simulation of turbulent flows. *J. Comp. Phys.* **151**, 757–789.

Loulou, P., Moser, R. D., Mansour, N. N. & Cantwell, B. J. 1997 Direct numerical simulation of incompressible pipe flow using a B-spline spectral method. *Technical Memorandum 110436*. NASA Ames Research Center.

Rhodes, Jr., E. J., Kosovichev, A. G., Schou, J., Scherrer, P. H. & Reiter, J. 1997 Measurements of frequencies of solar oscillations from the MDI medium-l program. *Solar Phys.* **175**, 287–310.

Stein, R. F. & Nordlund, A. 2000 Realistic solar convection simulations. *Solar Phys.* **192**, 91–108.

Werne, J., Birch, A. & Julien, K. 2004 The need for control experiments in local helioseismology. In *Proceedings of the SOHO14/GONG 2004 Workshop*.